Qualitative control of undesired oscillations in a genetic negative feedback loop with uncertain measurements

Lucie Chambon, Ismail Belgacem, Jean-Luc Gouzé

Qualitative control of undesired oscillations in a genetic negative feedback loop with uncertain measurements ⋆

Lucie Chambon [a], Ismail Belgacem [b], Jean-Luc Gouzé [a]

[a] *Université Côte d'Azur, Inria, INRA, CNRS, Sorbonne Université, Biocore Team, Sophia Antipolis, France*

[b] *Mathematics and Statistics, University of Victoria, PO BOX 1700 STN CSC, Victoria, B.C., Canada V8W 2Y2*

Abstract

In the context of gene regulatory networks, a negative feedback loop is modeled by N-coupled ordinary differential equations. The resulting system is highly non-linear due to the use of smooth Hill functions. This classical dynamical system properly captures the two main biological behaviors arising from this type of recurrent network motif: homeostasis under global stability of the unique fixed point, and biochemical oscillations otherwise. When homeostatic conditions are disrupted, undesired sustained oscillations can appear. In this context, a biologically relevant control strategy is designed in order to suppress these undesirable oscillations. As biological measurement techniques do not provide a quantitative knowledge of the system, the control law is chosen piecewise constant and dependent on specific regions of the state space. Moreover, due to biological devices inaccuracies, the measurements are considered uncertain leading to regions in which the control law is undefined. Under appropriate conditions on the control inputs, successive repelling regions of the state space are determined in order to prove the global convergence of the system towards an adjustable zone around the fixed point. These results are illustrated with the well-known p53-Mdm2 genetic feedback loop.

Key words: Qualitative control; Discrete measurements; Nonlinear systems; Bio control; Feedback loops.

1 Introduction

Gene regulatory networks govern biological functions as a whole. A better understanding of their underlying mechanisms as well as new strategies for the control of their dynamics would lead to an improvement regarding diseases insights and pharmacological treatments [38]. A close observation of their structure shows that these complex networks display recurrent motifs of interconnections composed of a small number of genes, that often play central roles in biological functions [34]. Negative feedback loops are a good illustration of such vital building blocks. They are identified as essential for homeostasis [25] (a vital function that maintains relatively constant the biological internal operating conditions) and oscillatory behaviours [10].

An homeostasis disruption, called a dyshomeostasis, may result in the emergence of undesirable sustained oscillations. As an example, the well-known gene p53 [24], involved in apoptosis, has been shown to be tightly regulated in healthy organisms in order to prevent extreme expression levels, likely responsible for various neurodegenerative diseases [39] and early embryonic lethality [4]. At the neuron scale, periodic firing patterns with under- and overstimulations, probably caused by an underlying genetic dyshomeostasis [17], are known to be involved in various cerebral damages [22,16]. Finding an appropriate way to tightly control and redesign these disrupted genetic systems is of really high interest.

To that end, synthetic biology has made significant progress in the recent years and has provided more and more control tools. In addition to classical approaches, such as inducer molecules introduction [32,14,15] and environmental disruptions [43], a more recent technique based on light pulses, called optogenetics, has been emerging [41,33]. However, it is important to keep in mind that all these synthetic techniques often lead to tedious and expensive experiments, partly due to the high precision and quality devices required, as well as the huge number of biological trials needed before developing the appropriate control. For all these reasons, the use of mathematical modeling and the theory of dynamical systems and control may provide a good insight in order to help designing the first draft of a control

⋆ This paper was not presented at any IFAC meeting. Corresponding author L. Chambon. Tel. +33492387174.

Email addresses: lucie.chambon@inria.fr (Lucie Chambon), ismailbelgacem@uvic.ca (Ismail Belgacem), jean-luc.gouze@inria.fr (Jean-Luc Gouzé).

strategy.

In order to stay as close as possible from the real biological context, the genetic dynamical model must be kept as exhaustive and general as possible, leading to the analysis of highly non-linear differential equations in which genes interactions are modeled by sigmoid Hill functions. These classes of systems are extensively used to model gene regulatory networks and properly describe transcriptional and translational genetic steps [20]. They are a generalization of Boolean genetic networks [40] and PWA systems [11]: even though they are more difficult to analyze, they keep exhaustive information and present less restrictive dynamics (see [8] for a review).

Regarding control, three main biological constraints must be considered. First, the nature of the inputs: biological control techniques, such as the one reviewed previously, often lead to constant inputs. Moreover, it often happens that the sign of the control law must be kept positive [21]. Second, the nature of the measurements: in biotechnology, quantitative measurements are mostly inaccessible. Indeed, measurement techniques such as fluorescence microscopy lead to a partial estimation of the temporal and spatial gene expression level within the cell. This biological reality prevents the implementation of classical control strategies that depend on precise and continuous knowledge of the state, and naturally encourages qualitative control depending on regions of the state space only. This class of control strategy has been already applied for different biological systems such as PWA gene regulatory networks. In [7] for example, the authors designed a qualitative control in order to globally stabilize the different fixed points of a two-dimensional PWA genetic positive feedback loop. This system was also controlled in [26] in order to stabilize its unstable fixed point, and real biological implementations were performed in order to support the analytical results. A similar idea is presented in [9], where the production rate of a two-dimensional PWA genetic feedback loop is controlled in order to create a periodic orbit. More theoretically, a general framework has been developed in [12] in order to control PWA gene regulatory networks. Third, uncertainties in the measurements: besides qualitative nature of measurements, inherent cells specificities and heterogeneities as well as limited sensitivity of measurement devices often induce noisy information. Uncertain control laws have been already applied for biochemical processes control strategies. In [28] for example, this type of control law has been designed in order to stabilize a working set point of a bioreactor and prevent washout.

These biological realities lead to the analysis of hybrid systems for which classical results about dynamics and control do not apply. For this purpose, new theory and new methods have been developed [27]. For hybrid systems with discontinuous right-hand sides in particular, the solutions can be defined with the theory of Filippov and differential inclusions [13], leading to specific dynamics such as sliding modes. The same limits occur when treating stability problems [36]. For example, the construction of smooth Lyapunov functions is a hard task for these types of systems [2]. Yet, few methods have been developed to answer stability questions for particular cases [5].

In this context, this paper presents a piecewise constant control strategy which considers the new synthetic control approaches as well as the three main biological constraints just presented, in order to recover the stable biological conditions of a disrupted negative feedback loop that exhibits undesired sustained oscillations.

The model of the negative feedback loop is presented in any dimension N with smooth non-linear Hill functions, and the piecewise constant control strategy leads to the analysis of a hybrid system with autonomous switch of its dynamics (Section 2). The construction of successive repelling regions allows to determine the qualitative dynamics of this system. It is shown that, under appropriate conditions on the control inputs, the sustained oscillations can be removed and the trajectories globally converge towards a small homeostatic zone (Section 3). Finally, this control strategy is illustrated with the well-known p53-Mdm2 negative feedback loop (Section 4).

2 Controlled negative feedback loop model

With N components, whether genes or proteins, the controlled negative feedback loop is described with the following system:

$$\begin{aligned} \dot{x}_1(x_1, x_N) &= \kappa_{01} + \mathrm{u}(x)\kappa_1 \mathrm{h}^-(x_N, \theta_N, n_N) - \gamma_1 x_1 \\ \dot{x}_i(x_i, x_{i-1}) &= \kappa_{0i} + \kappa_i \mathrm{h}^+(x_{i-1}, \theta_{i-1}, n_{i-1}) - \gamma_i x_i \end{aligned} \tag{1}$$

$\forall i \in \{2, .., N\}$, where

$$\begin{aligned} &\mathrm{u}(x) = u_{min} \ \forall x_1 \geq \bar{x}_1 + \delta_1, \\ &\mathrm{u}(x) = u_{max} \ \forall x_1 \leq \bar{x}_1 - \delta_1, \\ &\mathrm{u}(x) \in \{u_{min}, u_{max}\} \ \forall x_1 \in]\bar{x}_1 - \delta_1, \bar{x}_1 + \delta_1[. \end{aligned} \tag{2}$$

In a more compact form, this dynamical system can be noted $\dot{x} = F(\mathrm{u}(x), x)$. The functions $\mathrm{h}^+(x, \theta, n) = x^n/(\theta^n + x^n) \in [0, 1[$ and $\mathrm{h}^-(x, \theta, n) = 1 - \mathrm{h}^+(x, \theta, n) \in]0, 1]$ are sigmoid functions (called Hill functions) and respectively model activation and repression between variables with threshold θ and steepness n. These sigmoidal shape responses have been widely observed biologically and are a generalization of Michaelis-Menten kinetics for cooperative bindings: the parameter n is an integer that represents the number of transcription factors that need to bind to the promoter of the gene [20]. In addition, biological components are produced with a basal rate κ_{0i}, degraded with a rate γ_i and experience interaction with intensity κ_i. For biological consistency, all these parameters are considered strictly positive.

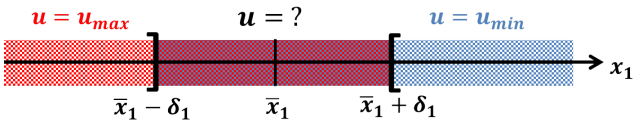

Fig. 1. The control takes the value u_{min} when $x_1 \geq \bar{x}_1 + \delta_1$, u_{max} when $x_1 \leq \bar{x}_1 - \delta_1$, and is undetermined when $\bar{x}_1 - \delta_1 < x_1 < \bar{x}_1 + \delta_1$.

In order to keep the biological experiments as simple as possible, the control law u(x) is arbitrarily dependent on the measurement of the first gene x_1 and acts on its own expression only. Moreover, the two constants u_{min} and u_{max} are adapted to the input types generated by biological control means. Finally, the measurements of x_1 are considered qualitative and uncertain, leading to partial knowledge of the system. The gene can either be detected highly expressed ($x_1 \geq \bar{x}_1$) or weakly expressed ($x_1 \leq \bar{x}_1$) and for a given measured x_1, the real system may be anywhere in the range $[x_1 - \delta_1, x_1 + \delta_1]$ where $2\delta_1 \geq 0$ models fluctuations, precision and sensibility of the measurement device [28]. As soon as x_1 in inside the uncertain domain $]\bar{x}_1 - \delta_1, \bar{x}_1 + \delta_1[$ (also called switching domain), the control law is undetermined and may either take the value u_{min} or u_{max} (see Fig. 1 for an illustration). Therefore, system (1) under unpredictable control law (2) is a differential system with discontinuous right-hand side and its solutions are appropriately defined in the sense of Filippov as the solutions of the following differential inclusion [13]:

$$\dot{x} \in H(x)$$

such that $H(x) = F(u_{min}, x)$ when $x_1 \geq \bar{x}_1 + \delta_1$, $H(x) = F(u_{max}, x)$ when $x_1 \leq \bar{x}_1 - \delta_1$ and

$$H(x) = \bar{co}\{F(u_{min}, x), F(u_{max}, x)\}$$

on the switching domain, where $\bar{co}$ is the closed convex hull of the set of vector field. These types of solutions often lead to the emergence of sliding modes along the switching domains.

When $u(x) = 1$, the usual negative feedback loop model is recovered and system (1) falls into the category of monotone cyclic feedback systems with a unique fixed point, called $\bar{x} = (\bar{x}_1, ..., \bar{x}_N)$. In dimension 2, the fixed point is globally asymptotically stable and appropriate conditions on the parameters can be determined for the emergence of damped oscillations. In dimension greater than 2 the dynamics is more complex, but a couple of results exist [29]. Depending on the parameters, two principal behaviours arise: global stability of $\bar{x}$ under sufficient conditions [1,37,44], and emergence of periodic solutions [23,19,31]. These two main dynamics properly capture the observed biological behaviours of negative feedback loops. It has been shown in the equivalent piecewise affine (PWA) systems that the emerging periodic orbit is unique and stable [11]. In this smooth non-linear version, the periodic orbit seems unique and globally attractive as well, but no rigorous proof of this observation exists.

Remark 1 *By studying the vector field, it is straightforward to show that system (1) with $u(x) = 1$ is a priori bounded: $x_1 \in]\kappa_{01}/\gamma_1, (\kappa_{01} + \kappa_1)/\gamma_1]$ and $x_i \in [\kappa_{0i}/\gamma_i, (\kappa_{0i} + \kappa_i)/\gamma_i[$ $\forall\, i \in \{2, .., N\}$.*

Hereafter, in the context of a disrupted homeostasis as presented in the introduction, the loop is supposed to be composed of at least three elements and the parameters of system (1) with $u(x) = 1$ are assumed to generate sustained oscillations: this dynamics is typically found with the fixed point $\bar{x}$ locally unstable. In order to remove the undesirable sustained oscillations, the control strategy (2) must lead to a global convergence of system (1) in a small region around the homeostatic state $\bar{x}$.

3 Global convergence

In this section it will be shown that, under appropriate conditions on the two constant inputs u_{min} and u_{max}, the homeostatic conditions are recovered. This will be proved by identifying specific dynamical transitions between zones of the state space. For this purpose, the space is partitioned as follows:

Definition 2 *The N-dimensional space is partitioned in 3^N zones. Each zone is called $(a_1 a_2 ... a_{N-1} a_N)$ such that $\forall i \in \{1, .., N\}$:*

- $a_i = 0$ *if* $x_i < \bar{x}_i - \nu_i$,
- $a_i = 1$ *if* $\bar{x}_i - \nu_i \leq x_i \leq \bar{x}_i + \delta_i$,
- $a_i = 2$ *if* $x_i > \bar{x}_i + \delta_i$,

where $\forall i \in \{2, .., N\}$:

- $\nu_1 = \delta_1$,
- $\delta_i = \left(\kappa_{0i} + \kappa_i h^+(\bar{x}_{i-1} + \delta_{i-1}, \theta_{i-1}, n_{i-1})\right)/\gamma_i - \bar{x}_i$,
- $\nu_i = \bar{x}_i - \left(\kappa_{0i} + \kappa_i h^+(\bar{x}_{i-1} - \nu_{i-1}, \theta_{i-1}, n_{i-1})\right)/\gamma_i$.

An illustration of the partitioning in dimension 3 is presented in Fig. 2.

Remark 3 *The term region will further refer to a union of zones. For example the region $a_1 = 2$ is the union of 3^{N-1} zones: $(2a_2 ... a_{N-1} a_N)$ where $a_i \in \{0, 1, 2\}$ $\forall i \in \{2, .., N\}$.*

Definition 4 *A region of the state space is repellent if:*

- *for each trajectory starting in this region, there is a time $T > 0$ after which the trajectory leaves the region,*
- *no trajectory enters this region.*

Practically, if the vector field $\dot{x}_i$ in a region $(a_1 ... a_N)$ keeps a non-zero constant sign in the whole region, including at the borders, the region is repelling in direction

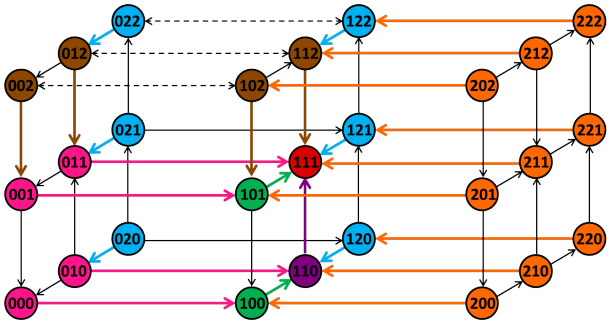

Fig. 2. Partitioning of the state space in dimension 3 according to Definition 2, and graph of transitions. The space is split in different zones of dimension 3 all represented as nodes in this figure. The arrows represent transitions between zones. Some transitions represented here by the plain black arrows do not play any role in the construction of the proof of Theorem 10. Moreover, because of the condition on u_{max}, some transitions (represented by dashed black lines) are undetermined. The successive repelling regions stated in Theorem 10 are represented with different colors. In the end, the trajectories converge towards the red zone (111).

i. When the region is upper (resp. lower) bounded in direction i, if $\dot{x}_i > 0$ (resp. $\dot{x}_i < 0$), the trajectories will leave the region through the upper (resp. lower) bound defining a_i.

The following conditions on u_{min} and u_{max} allow the statement of four Lemmas that successively define repelling regions of the state space:

Assumption 5 *With $\delta_1 \leq \bar{x}_1 - \kappa_{01}/\gamma_1$:*

$$u_{min} \leq \frac{\gamma_1(\bar{x}_1 + \delta_1) - \kappa_{01}}{\kappa_1},$$
$$u_{max} \geq \frac{\gamma_1(\bar{x}_1 - \delta_1) - \kappa_{01}}{\kappa_1 h^-(\bar{x}_N + \delta_N, \theta_N, n_N)}.$$

Lemma 6 *Under Assumption 5, the region defined by $a_1 = 2$ is repellent.*

PROOF. *It is shown that the region $a_1 = 2$ is repellent in direction 1, namely $\dot{x}_1 < 0$ in the whole region.*
For $x_1 > \bar{x}_1 + \delta_1$ the x_1-vector field is defined as: $\dot{x}_1(x_1, x_N) = \kappa_{01} + u_{min}\kappa_1 \mathrm{h}^-(x_N, \theta_N, n_N) - \gamma_1 x_1$. By evaluating this expression at the boundary $x_1 = \bar{x}_1 + \delta_1$ and using Assumption 5 on u_{min}, the following inequality comes up: $\dot{x}_1(\bar{x}_1 + \delta_1, x_N) \leq [\kappa_{01} - \gamma_1(\bar{x}_1 + \delta_1)]\left(1 - \mathrm{h}^-(x_N, \theta_N, n_N)\right)$. The bounded properties of system (1) with $u(x) = 1$ explained in Remark 1 give $\bar{x}_1 \in]\kappa_{01}/\gamma_1, \kappa_{01} + \kappa_1/\gamma_1]$ and by definition $\mathrm{h}^-(x_N, \theta_N, n_N) \in]0, 1]$. This implies $\dot{x}_1(\bar{x}_1 + \delta_1, x_N) \leq 0$. Moreover, for x_N fixed and $x_1 > \bar{x}_1 + \delta_1$, the linear degradation term $-\gamma_1 x_1$ in the x_1-vector field expression gives: $\dot{x}_1(x_1, x_N) < \dot{x}_1(\bar{x}_1 + \delta_1, x_N) \leq 0$. Hence, $\dot{x}_1(x_1, x_N) < 0 \ \forall \ x_N \geq 0$ and $\forall \ x_1 > \bar{x}_1 + \delta_1$. Finally, as $a_1 = 2$ is lower-bounded by $x_1 = \bar{x}_1 + \delta_1$, the region is repellent in direction 1. □

This first Lemma is illustrated in the left plot of Fig. 3 by the three blue arrows.

Lemma 7 *For any $i \in \{1, .., N-1\}$, the region defined by $a_i \in \{0, 1\} \cup a_{i+1} = 2$ is repellent.*

PROOF. *It is shown that for any $i \in \{1, .., N-1\}$, the region $a_i \in \{0, 1\} \cup a_{i+1} = 2$ is repellent in direction $i + 1$, namely $\dot{x}_{i+1} < 0$ in the whole region.*
By evaluating the x_{i+1}-vector field at the boundary $x_{i+1} = \bar{x}_{i+1} + \delta_{i+1}$ and using the definition of δ_{i+1}, the following inequality comes up: $\dot{x}_{i+1}(\bar{x}_{i+1} + \delta_{i+1}, x_i) = \kappa_{i+1}\left(\mathrm{h}^+(x_i, \theta_i, n_i) - \mathrm{h}^+(\bar{x}_i + \delta_i, \theta_i, n_i)\right)$. Moreover, in the relevant region, $x_i \leq \bar{x}_i + \delta_i$ leading to $\dot{x}_{i+1}(\bar{x}_{i+1} + \delta_{i+1}, x_i) \leq 0 \ \forall x_i \leq \bar{x}_i + \delta_i$. For any $x_{i+1} > \bar{x}_{i+1} + \delta_{i+1}$ and x_i fixed, the linear degradation term $-\gamma_{i+1}x_{i+1}$ in the x_{i+1}-vector field expression gives: $\dot{x}_{i+1}(x_{i+1}, x_i) < \dot{x}_{i+1}(\bar{x}_{i+1} + \delta_{i+1}, x_i) \leq 0$. Hence, $\dot{x}_{i+1}(x_{i+1}, x_i) < 0 \ \forall \ x_i \leq \bar{x}_i + \delta_i$ and $\forall \ x_{i+1} > \bar{x}_{i+1} + \delta_{i+1}$. Finally, as $a_i \in \{0, 1\} \cup a_{i+1} = 2$ is lower-bounded by $x_{i+1} = \bar{x}_{i+1} + \delta_{i+1}$, the region is repellent in direction $i + 1$. □

The two blue arrows in the right plot of Fig. 3 illustrate this second Lemma.

Lemma 8 *Under Assumption 5, the region defined by $a_N \in \{0, 1\} \cup a_1 = 0$ is repellent.*

PROOF. *It is shown that the region $a_N \in \{0, 1\} \cup a_1 = 0$ is repellent in direction 1, namely $\dot{x}_1 > 0$ in the whole region.*
For $x_1 < \bar{x}_1 - \delta_1$ the x_1-vector field is defined as: $\dot{x}_1(x_1, x_N) = \kappa_{01} + u_{max}\kappa_1 \mathrm{h}^-(x_N, \theta_N, n_N) - \gamma_1 x_1$. By evaluating this expression at the boundary $x_1 = \bar{x}_1 - \delta_1$ and using Assumption 5 on u_{max}, the following inequality comes up: $\dot{x}_1(\bar{x}_1 - \delta_1, x_N) \geq$

$$(\gamma_1(\bar{x}_1 - \delta_1) - \kappa_{01})\left[\frac{\mathrm{h}^-(x_N, \theta_N, n_N)}{\mathrm{h}^-(\bar{x}_N + \delta_N, \theta_N, n_N)} - 1\right].$$

Moreover, in the relevant region, $x_N \leq \bar{x}_N + \delta_N$, and Assumption 5 gives $\gamma_1(\bar{x}_1 - \delta_1) \geq \kappa_{01}$, leading to $\dot{x}_1(\bar{x}_1 - \delta_1, x_N) \geq 0 \ \forall \ x_N \leq \bar{x}_N + \delta_N$. For any $x_1 < \bar{x}_1 - \delta_1$ and x_N fixed, the linear degradation term $-\gamma_1 x_1$ in the x_1-vector field expression gives: $\dot{x}_1(x_1, x_N) > \dot{x}_1(\bar{x}_1 - \delta_1, x_N) \geq 0$. Hence, $\dot{x}_1(x_1, x_N) > 0 \ \forall \ x_N \leq \bar{x}_N + \delta_N$ and $\forall \ x_1 < \bar{x}_1 - \delta_1$. Finally, as $a_1 = 0$ is upper-bounded by $x_1 = \bar{x}_1 - \delta_1$, the region is repellent in direction 1. □

The two red arrows in the left plot of Fig. 3 illustrate this third Lemma.

Lemma 9 *For any $i \in \{1, .., N-1\}$, the region defined by $a_i \in \{1, 2\} \cup a_{i+1} = 0$ is repellent.*

PROOF. *It is shown that for any $i \in \{1, .., N-1\}$, the region $a_i \in \{1, 2\} \cup a_{i+1} = 0$ is repellent in direction $i + 1$, namely $\dot{x}_{i+1} > 0$ in the whole region.*

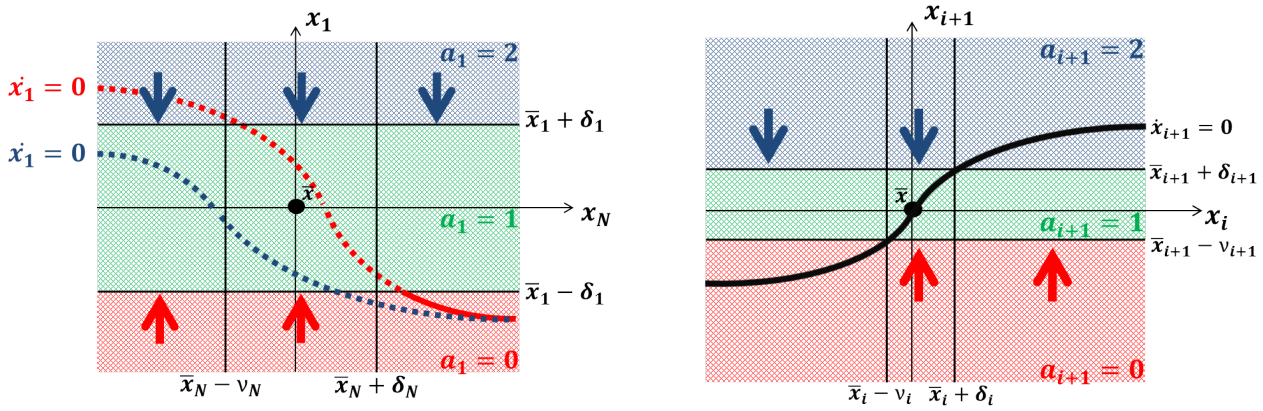

Fig. 3. Left: Transitions properties in the (x_1, x_N) plane. The dashed blue line is the x_1-nullcline for the region $a_1 = 2$. The half-plain half-dashed red line is the x_1-nullcline for the region $a_1 = 0$. The dashed style corresponds to nullclines situated in another region, and the plain style for nullclines situated in their proper region. There are no nullclines in the region $a_1 = 1$ as the control is undetermined. The arrows represent vector field in x_1-direction. Lemma 6 is illustrated by blue arrows, and Lemma 8 by red arrows. Right: Transitions properties in the (x_i, x_{i+1}) plane. The black line is the x_{i+1}-nullcline. The arrows represent vector field in x_{i+1}-direction. Lemma 7 is illustrated by blue arrows, and Lemma 9 by red arrows.

The argumentation follows the same structure as the proof of Lemma 7 by reversing all the inequalities and replacing all $+\delta$ by $-\nu$, giving: $\dot{x}_{i+1}(x_{i+1}, x_i) > 0 \ \forall \ x_i \geq \bar{x}_i - \nu_i$ and $\forall \, x_{i+1} < \bar{x}_{i+1} - \nu_{i+1}$. Finally, as $a_{i+1} = 0$ is upper-bounded by $x_{i+1} = \bar{x}_{i+1} - \nu_{i+1}$, the region is repellent in direction $i + 1$. □

This final Lemma is illustrated by the two red arrows in the right plot of Fig. 3. These four Lemmas finally allow the statement of the main result of this paper:

Theorem 10 *If Assumption 5 holds, system (1) under control law (2) converges globally towards the zone* $(a_1 ... a_N) = (1...1)$ *where* $a_i = 1 \ \forall i \in \{1, .., N\}$.

PROOF. As a base case, Lemma 6 states that any trajectory ends up in the region $a_1 \in \{0, 1\}$ (illustrated by the orange arrows in Fig. 2). Through an immediate mathematical induction, Lemma 7 states that any trajectory is further contained in the region $a_i \in \{0, 1\}$ $\forall i \in \{1, .., N\}$ (illustrated by the blue arrows, followed by the brown arrows in Fig. 2). As a new base case Lemma 8 states that any trajectory stands in the region $a_i \in \{0, 1\} \cup a_1 = 1 \ \forall i \in \{2, .., N\}$ (illustrated by the pink arrows in Fig. 2). Finally, by a second immediate mathematical induction, Lemma 9 states that any trajectory ends up in the zone $a_i = 1 \ \forall i \in \{1, .., N\}$ (illustrated by the green arrows, followed by the purple arrow in Fig. 2). In other words, the system is trapped in the zone $a_i = 1 \ \forall i \in \{1, .., N\}$, ending the proof of global convergence. □

This type of demonstration has been already exploited for similar systems [42,35,3,11]. In this paper however, the analysis intentionally considers a restricted number of transitions (colored arrows in Fig. 2) in comparison with classical proofs that analyze all potential transitions (supplementary black arrows in Fig. 2). While the traditional method gives more material about trajectories, this reduced approach greatly facilitates the understanding of the global dynamics in any dimension N.

Due to the unpredictable control law in the switching domain and the borders of the defined zones, some transitions are not unidirectional: in this case, the border of the two adjacent zones may be crossed in both directions (dashed black arrows in Fig. 2). This means that some cycles may emerge *between zones* (see for example the cycle 102 → 112 → 012 → 002 → 102 in Fig. 2). However, these cycles are not *periodic trajectories* (for the latter example, the variable x_3 decreases until the trajectory leaves the brown region).

Remark 11 *With the condition* $\delta_1 > \bar{x}_1 - \kappa_{01}/\gamma_1$, *the result is the same and the proof is straightforward. In this case, the value given to* u_{max} *has no influence on the invariant zone. Indeed, the region* $a_1 = 0$ *is naturally repellent as explained in Remark 1. In other words,* $u_{max} = 1$ *is enough to guarantee convergence towards* $(1...1)$. *This control strategy simplifies the biological set-up as* $u_{max} = 1$ *is equivalent to no control, inducing that the system must only be controlled in the half space* $x_1 \geq \bar{x}_1$.

This theoretical control strategy has a few convenient biological properties.

First, the switch between the two positive constants u_{min} and u_{max} may be biologically applicable with optogenetics or with the introduction of doses of inducer molecules for example, as long as the following method is applied: when the first gene x_1 is detected highly (resp. weakly) expressed compared to its normal homeostatic conditions, its inhibition by the last gene x_N must be reduced (resp. amplified).

Second, as long as u_{min} and u_{max} meet Assumption 5, the global convergence towards the attractive zone is

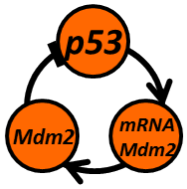

Fig. 4. The three components of the p53-Mdm2 negative feedback loop

still guaranteed, even if they fluctuate over time. This allows uncertainties and variations in the biological control input.

Third, this control approach guarantees convergence towards a region around $\bar{x}$. This small domain is satisfactory as strict convergence is not likely to occur in biology due to inherent and devices uncertainties. Theoretically, the boundaries of this convergence area may be tuned as close as desired from $\bar{x}$ by restricting the zone of fluctuation $2\delta_1$: indeed as δ_1 converges towards zero, the region shrinks around $\bar{x}$. In the case of perfect measurements, namely $\delta_1 = 0$, it is possible to show that $\bar{x}$ becomes a globally asymptotically stable fixed point of this ideal system. This result does not seem straightforward as $\bar{x}$ is neither a fixed point of the system controlled by u_{max} nor of the system controlled by u_{min}. One must keep in mind that these types of switching systems are not classic continuous dynamical systems and that more complex dynamical behaviors may happen. The theory of Filippov enables to show that the convergence arises through an "artificial" sliding mode along the hyperplane $x_1 = \bar{x}_1$, due to the opposite sign of the x_1 vector-field on both sides of the switching domain [13,5].

Importantly, this control strategy applies to a more general structure of negative circuits. Indeed, system (1) with $u(x) = 1$ can be seen as the canonical form of genetic negative loops: it is possible to show that any loop composed of an odd number of inhibitions (modeled by the decreasing Hill functions $h^-(.)$) is equivalent to system (1) after a change of variable (for example a loop composed of three genes that repress each other in dimension 3). Consequently, all these similar systems have exactly the same dynamics and the same properties, and it follows that control law (2) perfectly applies to them.

Next section illustrates this control strategy with the well-known p53-Mdm2 biological negative feedback loop.

4 A biological example: the p53-Mdm2 negative loop

The protein p53 plays an essential role in living organisms (see for example [24] for a complete review). In healthy and unstressed conditions, this protein is kept at low levels thanks to tight homeostatic control mechanisms [4]. In various stressed conditions however, such as the presence of malignant cells or in case of DNA damages, it has been observed that the concentration of p53 starts to oscillate [30].

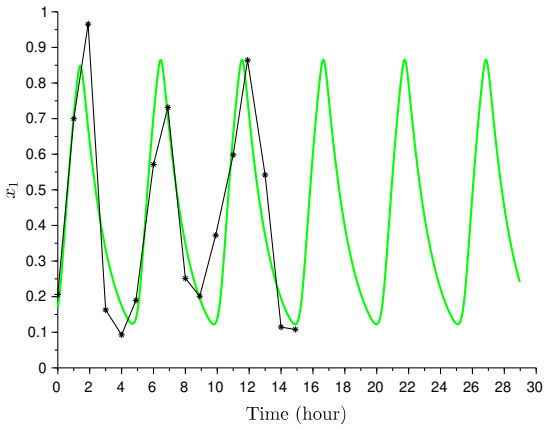

Fig. 5. The black star-plain line represents the p53-Mdm2 data from [18]. The green plain line is a simulation of system (1) with $u(x) = 1$, where the parameters are determined thanks to a least square routine in Scilab with symmetrical hypothesis: $\kappa_{0i} = 0.001$, $\kappa_i = 0.95$, $\gamma_i = 0.65$, $\theta_i = 0.49$ and $n_i = 10$ for $i \in \{1, 2, 3\}$.

These two main dynamical behaviors have been partly explained through a negative regulation of p53 by another protein called Mdm2. Several models have been built in order to recover these different observations (see for example [18] for a review). Among these possible models, one is similar to model (1) presented in section 2 with x_1 representing the concentration of p53, x_2 the concentration of a precursor of Mdm2, such as Mdm2 mRNA (messenger RNA), and x_3 the concentration of the protein Mdm2. The protein p53 is known to enhance the production of Mdm2 mRNA, itself enhancing the production of the protein Mdm2, and this latter inhibits the production of p53 as explained previously (see Fig. 4).

Importantly, it has also been recently observed that, due to its important role in apoptosis, inappropriate activity of p53 with too high or too low concentrations can lead to various diseases, such as neurodegenerative disorders characterized by a neuronal loss like Alzheimer [39], or early embryonic lethality [4]. In this context, the control strategy presented in this paper may be a useful tool in order to force a disrupted p53-Mdm2 loop that exhibits extreme undesirable values of p53 to recover healthy homeostatic conditions.

The oscillating p53 data points provided by [18] are fitted thanks to a least square method [1] with the classical cost function: $J(p) = \sum_{i=1}^{m} (x_1(t_i, p) - y_i)^2$, where m

[1] performed with Scilab: https://www.scilab.org/fr. Codes available upon request.

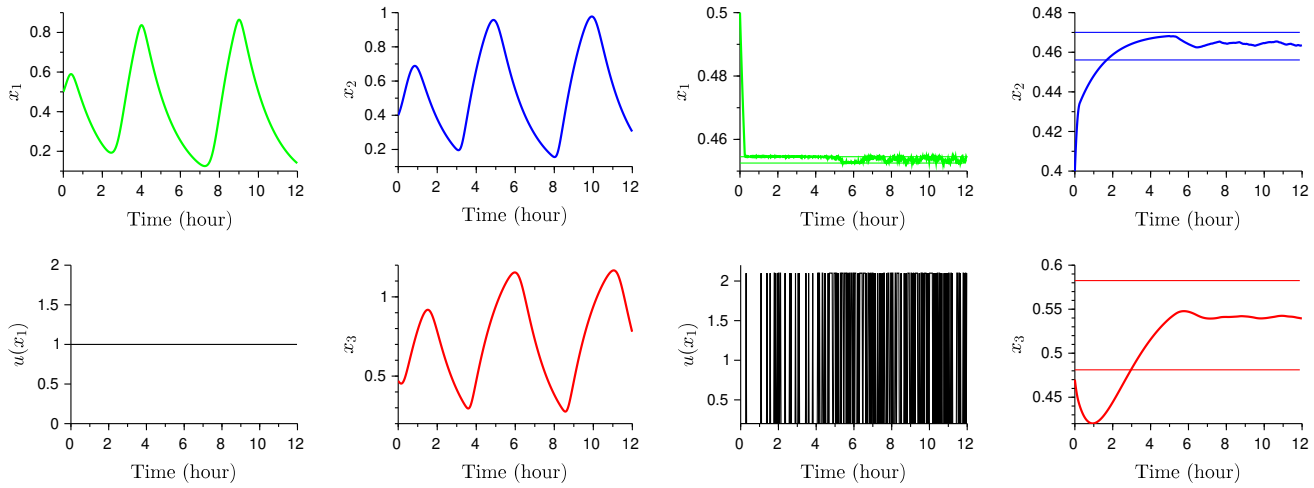

Fig. 6. For all plots, the parameters are the same as in Fig. 5. The trajectory for each variable is depicted with different colors (x_1: green, x_2: blue, x_3: red) and the black color is dedicated to the control law u(x). The four left plots represent a simulation of the uncontrolled system (1) with initial conditions $x_0 = (0.5, 0.4, 0.47)$: the three variables oscillate around the fixed point $\bar{x} = (0.45, 0.46, 0.53)$ and the control is fixed to 1. The four right plots represent a simulation of system (1) with same initial conditions x_0, under control law (2) with $\delta_1 = 0.001$, $u_{min} = 0.2$ and $u_{max} = 2.1$. As predicted, the trajectories converge towards the globally attractive zone defined with $\delta_2 \approx \nu_2 \approx 0.007$ and $\delta_3 \approx \nu_3 \approx 0.05$ represented by colored bands. As $x_1 \geq \bar{x}_1 + \delta_1$ initially, the control stays constant to u_{min} for a very short period of time. As soon as x_1 arrives in the unpredictable zone, the control starts switching stochastically between u_{min} and u_{max} with the same probability.

is the number of time points, y_i is the fluorescence measurement at time t_i provided by the data, and $x_1(t_i, p)$ is the evaluation of the first variable of the uncontrolled model (1) with the vector of parameters p. For sake of simplicity, the model is supposed to be symmetric: the parameters κ_{0i}, κ_i, θ_i, n_i and γ_i are supposed to be equal for any $i \in \{1, 2, 3\}$. In the end, the vector of parameters p contains 5 unknowns: $p = (\kappa_0, \kappa, \theta, n, \gamma)$. A last constraint consists in imposing n as an integer as explained in section 2. The result of this calibration is shown in Fig. 5.

The four left plots of Fig. 6 present a simulation of this uncontrolled fitted model with sustained oscillations. With a measurement error arbitrarily fixed to $\delta_1 = 0.001$, it is possible to observe in the four right plots of Fig. 6 that the control strategy presented in this paper induces a global convergence towards the analytic attractive zone (111) around the unstable fixed point, preventing unsafe extreme concentrations of p53. The convergence of the attractive zone towards $\bar{x}$ when $\delta_1 \to 0$, as discussed in the previous section, is illustrated in Fig. 7. This graph can be used in order to estimate the measurement precision needed for a desired convergence result.

It is possible to observe that the time step needed for the numerical resolution of the ODE produces a thicker convergence band than the one predicted for the first variable (see the top third plot of Fig. 6). This illustrates the fact that if the controller is limited in speed or if the measurements are slow compared to the time evolution of the system, the convergence result is no longer accurate. In this case, the boundaries of the convergence region would be fuzzier and a detailed study of this situation might be an interesting extension of the work.

As a remark, simulations need a probability distribution for the control in the region $a_1 = 1$ as it may take any of the two values u_{min} and u_{max}. As no a priori probability is evident about fluctuations in the measures, the numerical results are presented here with a classical discrete uniform distribution: the probability $p(.)$ that the control takes the value u_{min} is the same as the probability that the control takes the value u_{max}: $p(u_{min}) = p(u_{max}) = 0.5$. Another choice would have been to consider a spatially dependent control law where the probability depends on the distances to the boundaries $\bar{x}_1 - \delta_1$ and $\bar{x}_1 + \delta_1$. For a fixed x_1 in the uncertain zone, the probability $p(.|x_1)$ that the control takes the value u_{min} becomes $p(u_{min}|x_1) = \frac{1}{2\delta_1}(x_1 - \bar{x}_1) + \frac{1}{2}$, and the probability that the control takes the value u_{max} is defined as $p(u_{max}|x_1) = 1 - p(u_{min}|x_1)$. Another really easy choice would have been to fix the control either to u_{min} or u_{max} in the whole switching domain. This hypothesis would have led to the convergence of each variable towards one of the two boundaries of the convergence region. However, this error measurement model is not really likely to happen. Obviously, this probability distribution choice is only needed for a simulation purpose and does not affect the zone of convergence determined analytically.

5 Conclusion

This paper dealt with the problem of removing undesirable sustained oscillations emerging from a negative

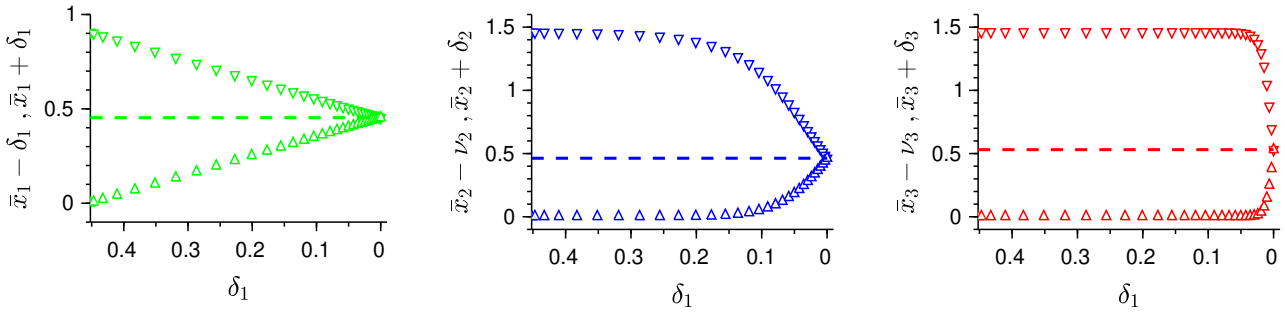

Fig. 7. Convergence of the attractive zone when δ_1 decreases from $\bar{x}_1 - \kappa_{01}/\gamma_1$ to 0. The parameters are the same as in Fig. 5. For each variable (x_1: green, x_2: blue, x_3: red), the upper bound $\bar{x}_i + \delta_i$ (resp. lower bound $\bar{x}_i - \nu_i$) is depicted with inverted (resp. upright) triangles. As explained, the convergence region shrinks around $\bar{x}$ (represented by dashed lines) as δ_1 tends to zero.

feedback loop in the context of homeostasis disruption within a gene regulatory network. The control strategy was designed in order to take into account three main biotechnological constraints. First, the qualitative nature of the measurements: in contrast with classical control theory, measures in biology are incomplete. Second, the qualitative nature of the inputs: whether optogenetics or classical introduction of chemicals often lead to discrete inputs. Third, uncertainties that often arise from measurements due to inherent stochastic properties of biological systems. From these three constraints, a qualitative control strategy was shown to lead to a global convergence towards a small zone around the unique unstable fixed point of the system, by determining a sequence of successive repelling regions.

This type of study can also be applied for the reverse problem: recover sustained oscillations in a disrupted negative feedback loop that shows either homeostatic conditions or perturbed oscillations. The control parameters can be tuned in order to fix the amplitude and the period of the clock. Our current work focuses on this idea and its application is interesting in the context of circadian rhythm disorders for example.

These types of control strategies can also be designed for other important genetic building blocks such as the toggle switch for example [26]. This motif is known to be essential for cell differentiation and cell decision making. Contrary to what may be believed, cell differentiation is a reversible process of really high interest nowadays due to the promising medical applications of stem cells. A qualitative control strategy can lead to a stabilization of the unstable fixed point, modeling a cell dedifferentiation process [6].

A more general framework may be developed in order to apply qualitative strategies to a large variety of gene regulatory networks [12]. From a defined qualitative measurement constraint, this framework may determine how and where to control the system in order to fulfill a convergence objective.

Acknowledgements

This work was supported by Région PACA and by the French Government (National Research Agency, ANR) through the "Investments for the Future" LABEX SIGNALIFE: program reference ANR-11-LABX-0028-01. The authors would also like to thank the reviewers for their constructive remarks.

References

[1] D. J. Allwright. A global stability criterion for simple control loops. *J. Math. Biology*, 4:363–373, 1977.

[2] A. Bacciotti and F. Ceragioli. Stability and stabilization of discontinuous systems and nonsmooth Lyapunov functions. *ESAIM: Control, Optimisation and Calculus of Variations*, 4:361–376, 1999.

[3] O. Bernard and J. L. Gouzé. Transient behavior of biological loop models with application to the Droop model. *Mathematical Biosciences*, 127:19–43, 1995.

[4] C. A. Brady and L. D. Attardi. p53 at a glance. *J Cell Sci*, 123(15):2527–2532, 2010.

[5] R. Casey, H. De Jong, and J. L. Gouzé. Piecewise-linear models of genetic regulatory networks: equilibria and their stability. *Journal of mathematical biology*, 52(1):27–56, 2006.

[6] L. Chambon and J. L. Gouzé. A new qualitative control strategy for the genetic toggle switch. *IFAC-PapersOnLine*, 52(1):532–537, 2019.

[7] M. Chaves and J. L. Gouzé. Exact control of genetic networks in a qualitative framework: The bistable switch example. *Automatica*, 47:1105–1112, 2011.

[8] H. De Jong. Modeling and simulation of genetic regulatory systems: a literature review. *Journal of computational biology*, 9(1):67–103, 2002.

[9] R. Edwards, S. Kim, and P. Van Den Driessche. Control design for sustained oscillation in a two-gene regulatory network. *Journal of mathematical biology*, 62(4):453–478, 2011.

[10] M. B. Elowitz and S. Leibler. A synthetic oscillatory network of transcriptional regulators. *Nature*, 403:335–338, 2000.

[11] E. Farcot and J. L. Gouzé. Periodic solutions of piecewise affine gene network models with non uniform decay rates: the case of a negative feedback loop. *Acta Biotheoretica*, 57:429–455, 2009.

[12] E. Farcot and J. L. Gouzé. Qualitative control of periodic solutions in piecewise affine models of genetic networks. *IFAC Proceedings Volumes*, 43(14):326–331, 2010.

[13] A.F. Filippov. *Differential Equations With Discontinuous Righthand Sides*. Kluwer, Dordrecht, The Netherlands, 1988.

[14] G. Fiore, G. Perrino, M. Di Bernardo, and D. Di Bernardo. In-vivo real-time control of gene expression: a comparative analysis of feedback control strategies in yeast. *ACS synthetic biology*, 5(2):154–162, 2015.

[15] C. Fracassi, L. Postiglione, G. Fiore, and D. Di Bernardo. Automatic control of gene expression in mammalian cells. *ACS synthetic biology*, 5(4):296–302, 2015.

[16] F. Fröhlich, M. Bazhenov, and T. J. Sejnowski. Pathological effect of homeostatic synaptic scaling on network dynamics in diseases of the cortex. *Journal of Neuroscience*, 28(7):1709–1720, 2008.

[17] F. Gachon, P. Fonjallaz, F. Damiola, P. Gos, T. Kodama, J. Zakany, D. Duboule, B. Petit, M. Tafti, and U. Schibler. The loss of circadian PAR bZip transcription factors results in epilepsy. *Genes & development*, 18(12):1397–1412, 2004.

[18] N. Geva-Zatorsky, N. Rosenfeld, S. Itzkovitz, R. Milo, A. Sigal, E. Dekel, T. Yarnitzky, Y. Liron, P. Polak, G. Lahav, and U. Alon. Oscillations and variability in the p53 system. *Molecular systems biology*, 2(1), 2006.

[19] L. Glass and J. S. Pasternack. Prediction of limit cycles in mathematical models of biological oscillations. *Bulletin of Mathematical Biology*, 40:27–44, 1978.

[20] B. C. Goodwin et al. *Temporal organization in cells. A dynamic theory of cellular control processes.* London and New York: Academic Press., 1963.

[21] F. Grognard, J. Rault, and J. L. Gouzé. Positive control for global stabilization of predator-prey systems. *IFAC Proceedings Volumes*, 46(23):265–270, 2013.

[22] D. Harnack, M. Pelko, A. Chaillet, Y. Chitour, and M. C.W. van Rossum. Stability of neuronal networks with homeostatic regulation. *PLoS computational biology*, 11(7):e1004357, 2015.

[23] S. Hastings, J. Tyson, and D. Webster. Existence of periodic solutions for negative feedback cellular control systems. *Journal of Differential Equations*, 25:39–64, 1977.

[24] E. R. Kastenhuber and S. W. Lowe. Putting p53 in context. *Cell*, 170(6):1062–1078, 2017.

[25] R. Lev Bar-Or, R. Maya, L. A. Segel, U. Alon, A. J. Levine, and M. Oren. Generation of oscillations by the p53-Mdm2 feedback loop: a theoretical and experimental study. *Proc Natl Acad Sci USA*, 97:11250–11255, 2000.

[26] J. B. Lugagne, S. Sosa Carrillo, M. Kirch, A. Köhler, G. Batt, and P. Hersen. Balancing a genetic toggle switch by real-time feedback control and periodic forcing. *Nature Communications*, 8:1671, 2017.

[27] J. Lunze and F. Lamnabhi-Lagarrigue. *Handbook of hybrid systems control: theory, tools, applications*. Cambridge University Press, 2009.

[28] F. Mairet and J. L. Gouzé. Hybrid control of a bioreactor with quantized measurements. *IEEE Transactions on automatic control*, 61(5):1385–1390, May 2016.

[29] J. Mallet-Paret and H. L. Smith. The Poincare-Bendixson theorem for monotone cyclic feedback systems. *Journal of Dynamics and Differential Equations*, 2:367–421, 1990.

[30] M. Maroto and N. Monk. *Cellular oscillatory mechanisms*, volume 641. Springer Science & Business Media, 2008.

[31] A. I. Mees and P. E. Rapp. Periodic metabolic systems: Oscillations in multiple-loop negative feedback biochemical control networks. *J. Math Biology*, 5:99–114, 1978.

[32] F. Menolascina, G. Fiore, E. Orabona, L. De Stefano, M. Ferry, J. Hasty, M. Di Bernardo, and D. Di Bernardo. In-vivo real-time control of protein expression from endogenous and synthetic gene networks. *PLoS computational biology*, 10(5), 2014.

[33] A. Milias-Argeitis, M. Rullan, S. K. Aoki, P. Buchmann, and M. Khammash. Automated optogenetic feedback control for precise and robust regulation of gene expression and cell growth. *Nature communications*, 7:12546, 2016.

[34] R. Milo, S. Shen-Orr, S. Itzkovitz, N. Kashtan, D. Chklovskii, and U. Alon. Network motifs: Simple building blocks of complex networks. *Science*, 298:824–827, Oct 2002.

[35] S. Pigolotti, S. Krishna, and M. H. Jensen. Oscillation patterns in negative feedback loops. *Proceedings of the National Academy of Sciences*, 104(16):6533–6537, April 2007.

[36] A. Polyakov and L. Fridman. Stability notions and Lyapunov functions for sliding mode control systems. *Journal of the Franklin Institute*, 351(4):1831–1865, 2014.

[37] L. A. Sanchez. Global asymptotic stability of the Goodwin system with repression. *Nonlinear Analysis: Real World Applications*, 10:2151–2156, 2009.

[38] E. D. Sontag. Molecular systems biology and control. *European journal of control*, 11(4-5):396–435, 2005.

[39] A. Szybińska and W. Leśniak. P53 dysfunction in neurodegenerative diseases-the cause or effect of pathological changes? *Aging and disease*, 8(4):506, 2017.

[40] R. Thomas and R. d'Ari. *Biological feedback*. CRC press, 1990.

[41] J. E. Toettcher, D. Gong, W. A. Lim, and O. D. Weiner. Light-based feedback for controlling intracellular signaling dynamics. *Nature methods*, 8(10):837–839, 2011.

[42] J. J. Tyson. On the existence of oscillatory solutions in negative feedback cellular control processes. *Journal of Mathematical Biology*, 1(4):311–315, 1975.

[43] J. Uhlendorf, A. Miermont, T. Delaveau, G. Charvin, F. Fages, S. Bottani, G. Batt, and P. Hersen. Long-term model predictive control of gene expression at the population and single-cell levels. *Proceedings of the National Academy of Sciences*, 109(35):14271–14276, August 2012.

[44] L. Wang, P. De Leenheer, and E. D. Sontag. Conditions for global stability of monotone tridiagonal systems with negative feedback. *Systems and Control Letters*, 59:130–138, 2010.